Journal of Power Sources 195 (2010) 1905–1913

Contents lists available at ScienceDirect

Journal of Power Sources

journal homepage: www.elsevier.com/locate/jpowsour

Load-following active power filter for a solid oxide fuel cell supported load

Allie E. Auld, Keyue M. Smedley, Fabian Mueller, Jack Brouwer*, G. Scott Samuelsen

Advanced Power and Energy Program, University of California, Irvine, CA 92697, United States

ARTICLE INFO

Article history:
Received 28 July 2009
Received in revised form 1 October 2009
Accepted 2 October 2009
Available online 9 October 2009

Keywords:
Active power filter
Distributed generation
Dynamic modeling
Load-following
One-cycle control
Solid oxide fuel cell

ABSTRACT

While the integration of base-load fuel cells into the built environment is expected to provide numerous benefits to the user, the steady-state and dynamic behavior of these stationary fuel cell systems can produce an undesirable impact on the grid distribution circuit at the point of connection. In the present paper, a load-following active power filter (LFAPF) is proposed to mitigate the grid impact of such systems and instead improve overall local power quality. To evaluate the strategy, the LFAPF is integrated into a SOFC system inverter with one-cycle control (OCC) to provide the fundamental benefits of a traditional active power filter (APF) while also damping out short-term line current transients. The LFAPF benefit is illustrated through simulation of an SOFC interconnected with the utility electric distribution system and a building electricity demand that is modeled as a dynamic non-linear load. Three installation cases are examined: (1) a load-following SOFC, (2) a base-loaded SOFC, and (3) an offline SOFC. Without LFAPF, the load-following SOFC causes load transients due to the finite SOFC response time, and the base-loaded SOFC case has transients that appear more severe because they represent a larger overall percentage of the grid-provided load. The integration of an LFAPF improves the steady-state behavior over the base case and mitigates voltage sags and step changes. Thus integrating an LFAPF can, by providing useful services to both the utility and the end-user, facilitate the integration of an SOFC into the distribution system.

1. Introduction

The commercial deployment of large fuel cells (>200 kW) is accelerating to provide base-load power for a variety of applications including hotels, universities, food processing and industrial facilities, and waste water treatment plants. In California, for example, over 25 MW of commercial molten carbonate fuel cell (MCFC) and phosphoric acid fuel cell (PAFC) products are installed. Other types of fuel cell systems are under development. In particular, a number of manufacturers are developing solid oxide fuel cell (SOFC) product for commercialization in the near future.

While much research and development has been occurring on alternative energy technologies, a key aspect of the successful widespread deployment of distributed generation (DG) is a robust grid interconnection. This grid interconnection should ideally be designed to maximize overall DG benefits, increase power reliability for the customer, and improve grid functionality for the utility. An interconnection that does not meet these goals will inevitably create a barrier to either utility or customer acceptance. It is therefore important to understand and optimize the interconnection of DG, load, and the electric utility.

Power quality is a major issue for customers and the utility due to the increasing penetration of electric loads that are sensitive to harmonics and fluctuations in voltage and frequency. Incidentally, many of these sensitive loads, which include computers, electronics, and processing machinery, are simultaneously responsible for creating problems with power quality [1]. Thus, the utility cannot take full responsibility for providing optimal power quality, as the problems for a customer may arise as a result of that very customer's own equipment. One illustrative example of this occurs during sudden load changes. Load increases and decreases may occur during the start and stop of a large load with cycling behavior, such as an air conditioning compressor motor or arc furnace [2]. A voltage sag can accompany a sudden surge of inrush current, which may disrupt functionality or cause failure in delicate equipment on a neighboring circuit. This voltage sag can be greatly reduced or eliminated by supplying this current at the site of the load instead, since the voltage drop occurs locally and cannot be easily addressed by the grid due to the line impedance of the electric power distribution system.

An existing solution to power quality problems is the active power filter (APF). APF technology can compensate for current harmonics, balance phases, and provide reactive power compensation [3]. An APF essentially turns an unbalanced non-linear "troublesome" load into one that appears extremely "clean" from the utility perspective. The one-cycle control (OCC) method has been used to design and build a robust, simple APF in [4]. The addition of an APF

* Corresponding author. Tel.: +1 949 824 1999; fax: +1 949 824 7423.
E-mail address: jb@nfcrc.uci.edu (J. Brouwer).

0378-7753/$ – see front matter © 2009 Elsevier B.V. All rights reserved.
doi:10.1016/j.jpowsour.2009.10.005

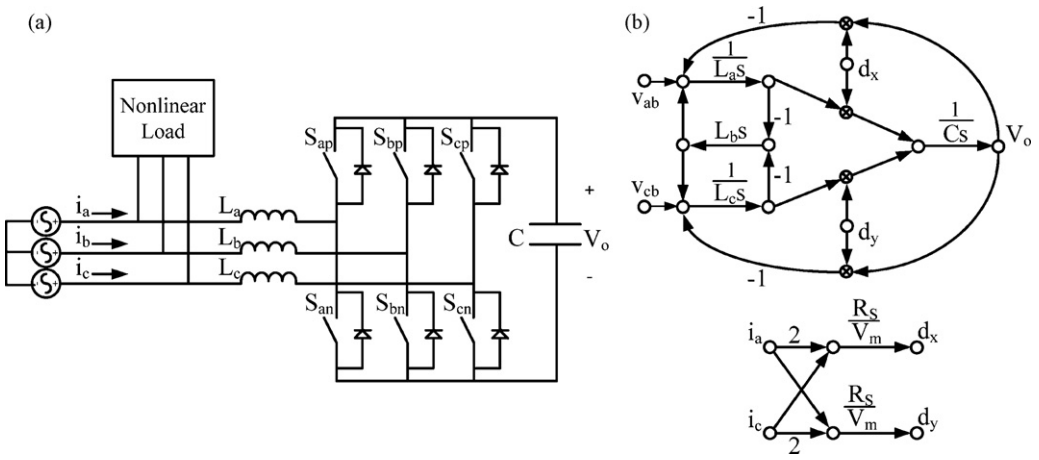

Fig. 1. OCC APF (a) power stage circuit diagram and (b) large-signal switching flow-graph model [6].

to the grid interconnection of a solid oxide fuel cell (SOFC) has been shown to allow the SOFC and inverter to supply grid-connected real power without perturbing the utility system by locally compensating for the harmonics and reactive power associated with practical building loads [5]. Thus, the APF provides benefits for power quality in the steady-state, but this does not guarantee that it will be effective for eliminating voltage sags or other transient-based power quality issues. The local DG could address the voltage sag issue by supplying power changes directly, but fuel cells lack the rotating inertia of large synchronous generators and are thus unable to buffer rapid load transients. Instead, the OCC APF is redesigned to provide local power buffering and thus provide dynamic protection against rapid voltage transients in addition to the established steady-state APF functions.

The two issues investigated in this paper are the APF capabilities in steady-state and load-following applications with an SOFC. The steady-state operation has already been verified in [6], but the control method is redesigned herein to allow for improvement of the dynamic operation to create a load-following active power filter (LFAPF). In Section 2, the benefits and theory of an OCC APF are summarized and dynamic models of the SOFC, inverter, and dynamic non-linear load are presented. In Section 3, the SOFC operation without APF is simulated. Section 4 expands on the model from Section 3 to demonstrate the operation of the LFAPF for the following conditions: (1) SOFC capable of load-following, (2) SOFC providing base-load power, and (3) SOFC offline (base case). A sensitivity analysis in Section 5 illustrates the dependence of the LFAPF overall effectiveness on the design parameters, and Section 6 presents the conclusions.

2. Dynamic physical models

2.1. Power electronics models

The two power electronics models used in this work are the one-cycle control (OCC) inverter and OCC APF. The description of the development and experimental verification of the OCC inverter is shown in [7], and the development, verification and application of the inverter model is described fully in [5,8,9]. The OCC APF design is originally developed and verified experimentally in [4,10,11], and the APF model is introduced in [6]. The OCC APF model uses the switching flow-graph method from [12], and is also incorporated with an inverter, SOFC, and load in [5]. The schematic of the power stage of the APF and the switching flow-graph model of the APF control are both presented in Fig. 1.

The overall control goal of the OCC APF is to maintain and match an input current to a reference voltage according to an emulated resistance. This control goal is shown in Eq. (1) where v_a, v_b, and v_c are the line voltages, i_a, i_b, and i_c are the grid currents, and R_e is the emulated resistance of the combination of the load and APF.

$$\begin{bmatrix} v_a \\ v_b \\ v_c \end{bmatrix} = R_e \cdot \begin{bmatrix} i_a \\ i_b \\ i_c \end{bmatrix} \tag{1}$$

The description of the OCC controller in [11] illustrates the entire 360° line cycle divided into 6–60° regions that can each be controlled by two active switch pairs, and the signals to each pair are complementary. Thus, for any region, the entire converter behavior can be defined by the duty ratios for two switches: d_p and d_n. The OCC controller uses the input voltages to select which switches are active and generates the duty ratios d_p and d_n by the key control Eq. (2), which is developed from the control goal (1) in [11].

$$V_m \cdot \begin{bmatrix} 1-d_p \\ 1-d_n \end{bmatrix} = R_S \cdot \begin{bmatrix} 2 & 1 \\ 1 & 2 \end{bmatrix} \cdot \begin{bmatrix} i_p \\ i_n \end{bmatrix} \tag{2}$$

R_s is the sensing resistance and i_p and i_n are selected input currents. V_m is a compensated feedback parameter that is defined by (3), where V_o is the voltage across the APF DC capacitor.

$$V_m = R_S \cdot \frac{V_o}{R_e} \tag{3}$$

The behavior of the APF can be controlled by the determination of V_m, which is calculated by comparing the APF capacitor voltage, V_o, to the desired capacitor voltage, V_{ref}, through a PI gain. The design objective of the load-following APF is to inhibit changes in the magnitude of the line current, not to necessarily keep the capacitor voltage at a set value. Thus the PI control in the LFAPF is set to low values, so that the APF will subsequently not prioritize maintaining the capacitor voltage. The default proportional and integral values are $P = 1$ and $I = 0.2$. To enhance the transient energy buffer capability of the LFAPF, the capacitor size can be increased to raise energy storage capability. The DC capacitor, C, has a default value of 300 mF, and the three inductors L_a, L_b, and L_c are each 0.5 mH.

2.2. SOFC

SOFC technology is a type of high temperature fuel cell that is currently the subject of active research, development and investment for distributed and central power generation applications [13–17].

The SOFC dynamic model resolves physical, chemical and electrochemical dynamics of a fuel cell system in Matlab/Simulink® in

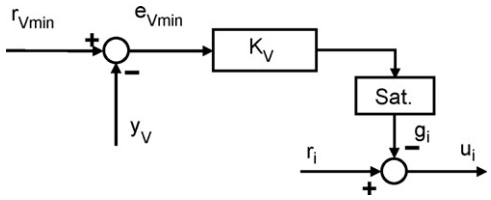

Fig. 2. Fuel depletion voltage feedback current governor.

a manner similar to that presented in [5,18]. The modeling methodology solves dynamic mass and energy conservation equations and heat transfer within the fuel cell and amongst SOFC system components, which are methods that have been extensively described and applied as presented in [19–27]. The methodology has compared favorably to experimental data from dynamic single cell transients [26], integrated simple cycle SOFC systems [19], SOFC-MTG hybrid systems [21], and proton exchange membrane stationary fuel cell systems [27]. The difference between the model used here and that of [5] is the method for approximating the fuel flow delay and the reference governor control strategy implemented to prevent fuel depletion in the anode compartment during transient operation. Results from [5] show that the fuel flow delay (associated with control, actuator (e.g., valve), reformer and other upstream component flow dynamics) strongly affects the SOFC system response to perturbations, and [28] shows that flow dynamics typically limit the SOFC inherent transient capability. Hence, the current model implements a more physically-based delay by modeling the fuel flow as the volumetric filling of a plenum volume and a flow restriction as was developed and explored in [29,30] and used to develop SOFC control strategies in [24,25,31]. The change in pressure of a plenum volume can be derived from the ideal gas law and is determined by the following equation:

$$\frac{dP}{dt} = \frac{RT}{V} \cdot (\dot{N}_{\text{ref}} - \dot{N}_{\text{SOFC}}) \tag{4}$$

The orifice equation is used to model the flow restriction between the fuel reformer and other upstream components and the fuel cell. This equation is a function of the pressure difference across the orifice, which is presented in (5), where ΔP is the pressure drop and K is a constant of the appropriate system components.

$$\dot{N}_{\text{SOFC}} = \frac{\sqrt{\Delta P}}{K} \tag{5}$$

The above equations are combined to form the single result presented in the following equation:

$$\frac{dP}{dt} = \frac{RT}{V}\left(\dot{N}_{\text{ref}} - \frac{\sqrt{\Delta P}}{K}\right) \tag{6}$$

The modeled volumetric flow rate into the anode compartment during a transient response to an increase in fuel demand agrees well with experimental results [29]. Fuel starvation in the anode compartment can occur if the fuel is consumed by the electrochemical reactions faster than it can be supplied by the fuel delivery system. This fuel starvation phenomenon is rapidly (at the speed of the electrochemical reactions) indicated by the voltage that the SOFC can sustain during transient operation. A minimum acceptable voltage level is applied to a fuel cell current governor to prevent fuel starvation as presented in Fig. 2, where r_{vmin} is the minimum voltage setpoint, y_v is the voltage measurement, r_i is reference current, K_v and Sat are feedback gain and saturation, and u_i is the input current. This type of governor is explored and discussed in detail in [31]. The voltage feedback current governor provides advantages over the utilization-based governor implemented in [5] that include: (1) eliminating the need to measure fuel flow rate, and (2) allowing fuel stored within the anode compartment to be consumed to maximize the transient load-following capability.

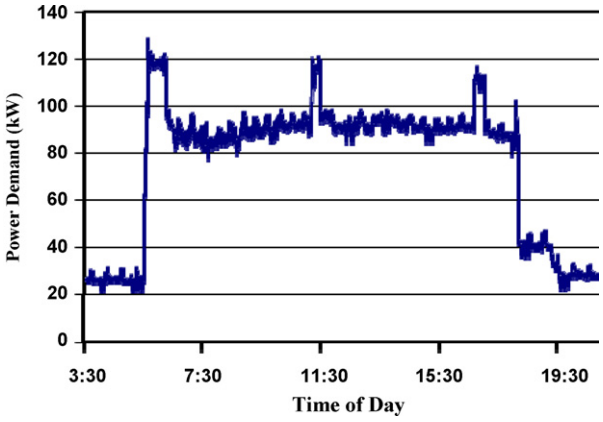

Fig. 3. Representative office building diurnal load profile.

2.3. Dynamic non-linear load

While load measurement and monitoring provides valuable insights into the behavior of real loads, the current draw of a dynamic non-linear load cannot be completely defined by direct measurement because the current depends upon the voltage in a generally non-linear way. The addition of local power generation or APF to the load will affect the local load voltage, and thus change the current as a result. Instead the load is approximated by looking at general trends and behaviors. As shown in [2], commercial office buildings tend to have two distinct load levels: off-use and on-use. The transition between the levels occurs in the early morning when the air conditioning system starts up to condition the building for the day. A similar decrease corresponds to the system shut down in the evening. A representative measured example of this behavior is presented in Fig. 3. The dynamic behavior of this commercial office building is concisely summarized and simplified as comprised of two different power levels with severe increase and decrease transients that each occur once per day. The time interval of this transition depends upon the specific characteristics of the air conditioning system and can vary from milliseconds for plain induction motors [32] to as long as 2–5 s for those with start-up control [33]. The faster transition time is selected in the present paper so that the techniques investigated can be applied to less severe systems.

The non-linear aspects of the load are simulated by a three-phase diode rectifier model that was originally developed for Matlab/Simulink® in [34]. A schematic of the diode rectifier and line impedance from [34] is presented in Fig. 4. The values used to simulate the rectifier behavior herein are, $L_f = 2$ mH, $R_f = 0$, $C_{\text{DC}} = 0.01$ F. The load transient is created by a step change in the DC-side power demand at a time of 1 s, which has power set points of

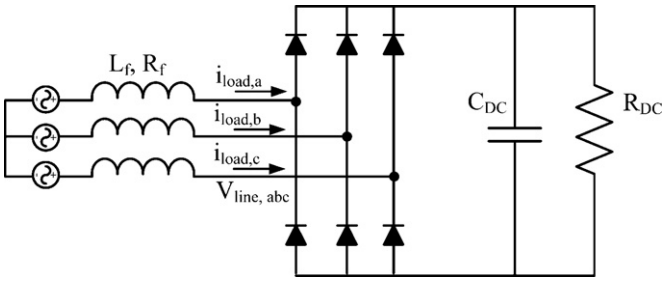

Fig. 4. Schematic of three-phase diode rectifier circuit.

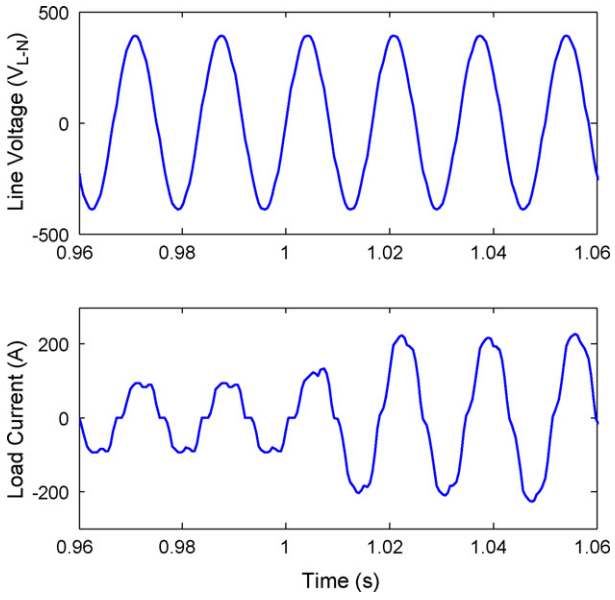

Fig. 5. Three-phase diode rectifier load during transient.

$P_{DC,initial}$ = 50 kW and $P_{DC,final}$ = 100 kW for the load increase condition, and reversed values for the load decrease condition. The voltage source is 60 Hz with a magnitude of 480 V_{L-L}. The measured line voltage and load current profile of phase A before, during, and after a transient increase is presented in the top and bottom of Fig. 5, respectively.

3. No APF case

The first case investigated is the connection of a load-following SOFC with inverter to a remote non-linear load without addition of an APF. The schematic of the system is shown in Fig. 6. P_{grid} is the desired amount of power imported from the grid, P_{load} is the amount of power drawn by the load, and $i_{inv,abc}$ are the three-phase currents provided by the SOFC/inverter system. $V_{load,abc}$ are the three-phase voltages at the load bus, and $i_{line,abc}$ are the three-phase currents supplied by the electric power system. The power demand, P_{demand}, is the load power minus the desired grid power. P_{grid} is set to 10 kW for this case. The line impedance located in Fig. 6 between the line and load voltage is 10% per-unit on a 100-kVA basis and the reactance is twice the resistance, which is typical of distribution line impedances.

The response of the SOFC to a step increase in load demand perturbation is presented in Fig. 7. The SOFC increases power output immediately due to stored fuel in the anode compartment, but

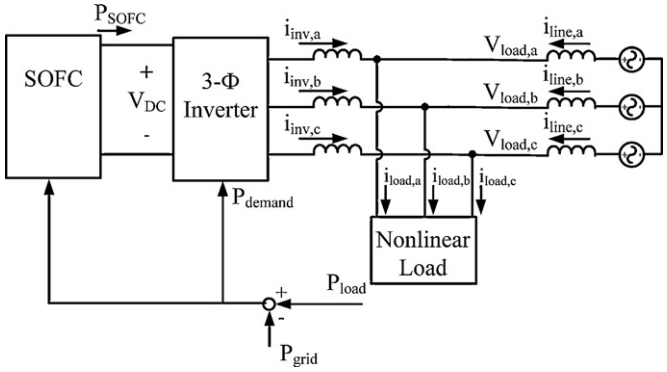

Fig. 6. Block schematic for SOFC/Inverter and non-linear load.

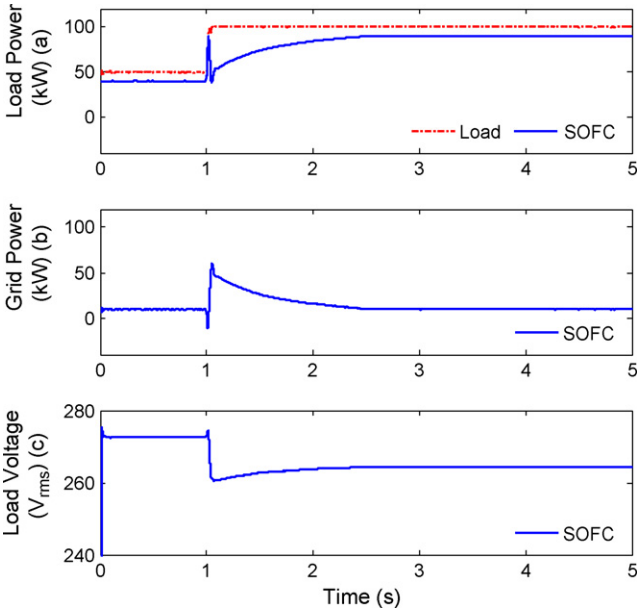

Fig. 7. Load-following capability of SOFC: (a) load and SOFC power, (b) grid power, and (c) load rms voltage.

power then falls sharply when the internally stored fuel is depleted. The power output then rises gradually to meet the new power demand as the fuel reaching the fuel cell increases. The area of energy shortfall between demand and SOFC output corresponds to increased power draw from the grid, which is presented at the middle of Fig. 7. The grid power increases from a steady 10 kW to as high as 60 kW during the transient period. This power increase is associated with a sag in the rms voltage that also occurs at the time of the perturbation (1 s), which is presented at the bottom of Fig. 7. The voltage recovers partially as the SOFC power output increases, but the final steady-state value remains below the initial value due to the load characteristics at the higher power level.

A close-up of the actual voltage and current waveforms for phase A is presented in Fig. 8. The distortion in the voltage waveform is due to the non-linear line current being drawn through the line impedance. The load current is non-linear because of the diode rectifier behavior. The inverter current waveform is designed to match the voltage waveform, which results in an essentially sinusoidal

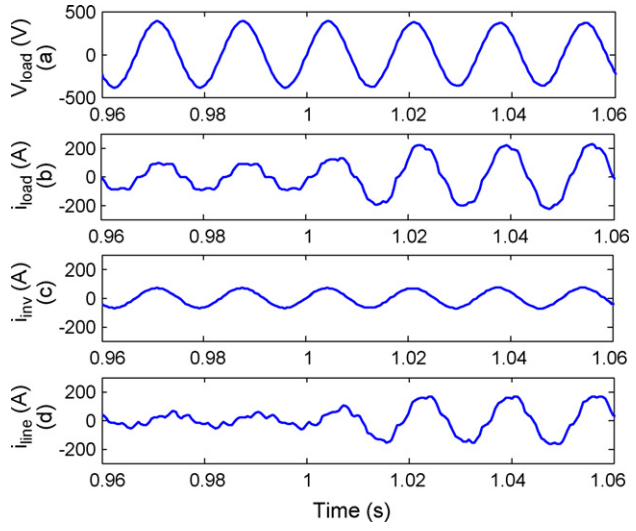

Fig. 8. No APF case: (a) load voltage, (b) load current, (c) inverter current, and (d) line current (phase A).

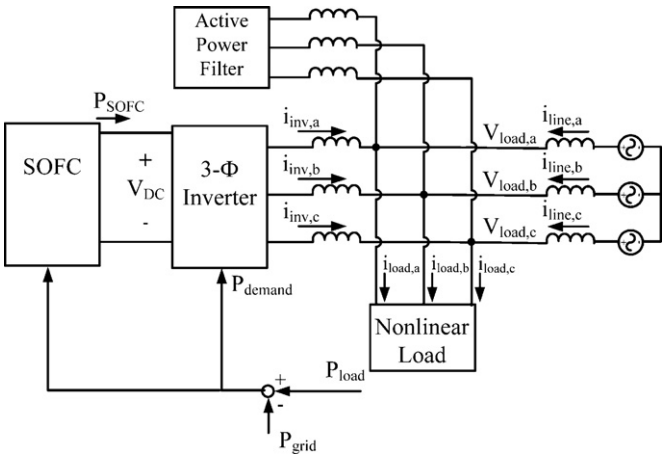

Fig. 9. Block schematic for load-following SOFC/inverter with LFAPF.

inverter current. The line current is the load current minus the inverter current. The inverter matches the fundamental frequency of the load current, but because the current harmonics associated with non-linearity of the load are not compensated, the line current has an extremely high percentage of harmonics.

4. Implementation of load-following APF

With the aim of improving steady-state and transient response, a load-following shunt APF is added to the circuit as shown in Fig. 9. The three SOFC cases simulated include a base-loaded SOFC, a load-following SOFC, and no SOFC. A base-loaded SOFC operates only at one set power output level, and is indicative of the current state of high temperature fuel cell systems. The load-following SOFC control measures the load power demand, subtracts the desired grid tie-line power, and then inputs the resulting power demand to the SOFC and inverter. A schematic of this control strategy is presented below in Fig. 9. The load-following SOFC is able to follow a changing power reference to meet the dynamic needs of the building. The case without an SOFC reflects the reality that DG system will need to be shut down periodically for scheduled or unscheduled maintenance and the behavior during these contingencies must still be acceptable.

4.1. Base-loaded SOFC

The model for the base-loaded SOFC case is the same dynamic model described in Section 2, except that the power demand is set as a constant 40 kW, which is less than the building minimum load as is currently required for many state grid interconnection laws. In the load-following SOFC case, the LFAPF provides energy storage to supplement a temporary power deficit of the SOFC system in response to a load increase perturbation. With a base-loaded SOFC, this energy storage instead simply smoothes out the transition between the two system states. Simulation results for the morning start-up transition between these two states are presented in Fig. 10, where the grid power for the SOFC-only case is a step power increase from 10 to 60 kW. Similarly, simulation results for the evening shut-down transient presented in Fig. 11 show responses to a step power decrease from 60 to 10 kW. In both cases, the addition of an LFAPF reduces the slope of this dynamic and causes the transition to take about 0.7 s for the morning start-up case and over 4 s in the evening shut-down case. In both cases, the slower transition also allows the local load voltage to change gradually, in contrast to the step voltage change exhibited by all cases without LFAPF.

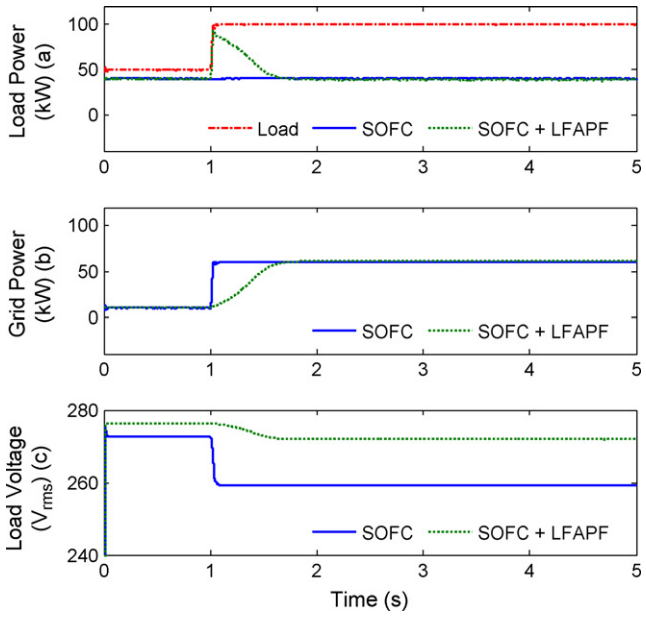

Fig. 10. Comparison of base-load SOFC with and without LFAPF during load increase.

When the SOFC power output does not change, but the load power demand does, fluctuating voltage and grid power demand is unavoidable without substantial energy storage. However, decreasing the severity of this transition provides a benefit for both the building load, by mitigating voltage variation, and the utility, by decreasing the system grid power ramp rate. The LFAPF is able to accomplish these functions with a modest amount of energy storage. Additionally, the steady-state voltage difference between light and heavy load is greatly reduced for the LFAPF case as well.

In addition to concerns over the dynamic voltage quality, the steady-state power quality is the traditional goal of APF implementation. Waveforms for phase A of the key voltage and currents are presented in Fig. 12. The LFAPF case line voltage waveform in Fig. 12a shows less distortion, which is caused by non-linear current, than the SOFC-only case in Fig. 8a. The LFAPF compensation

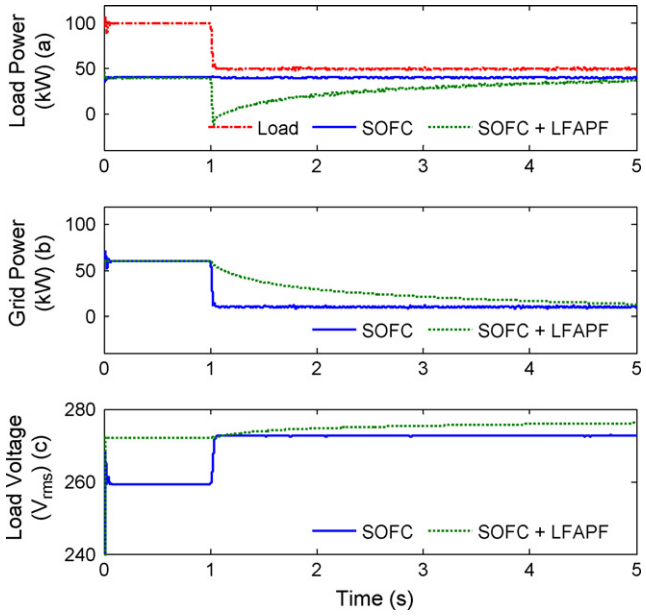

Fig. 11. Comparison of base-load SOFC with and without LFAPF during load decrease.

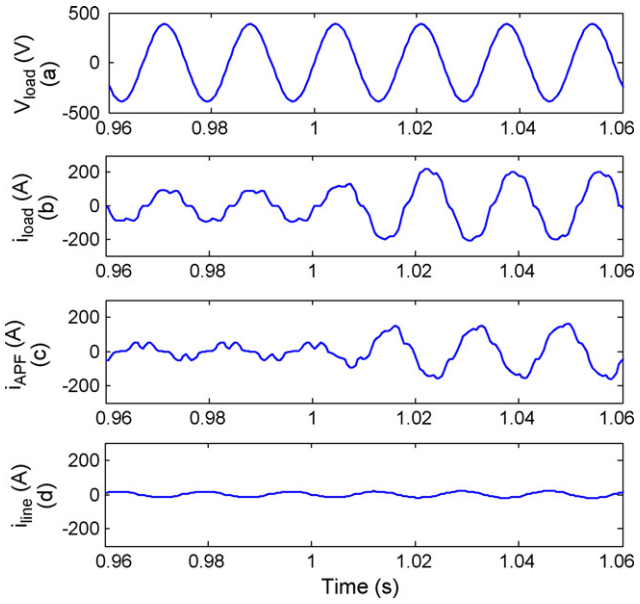

Fig. 12. LFAPF case: (a) load voltage, (b) load current, (c) inverter current, and (d) line current (phase A).

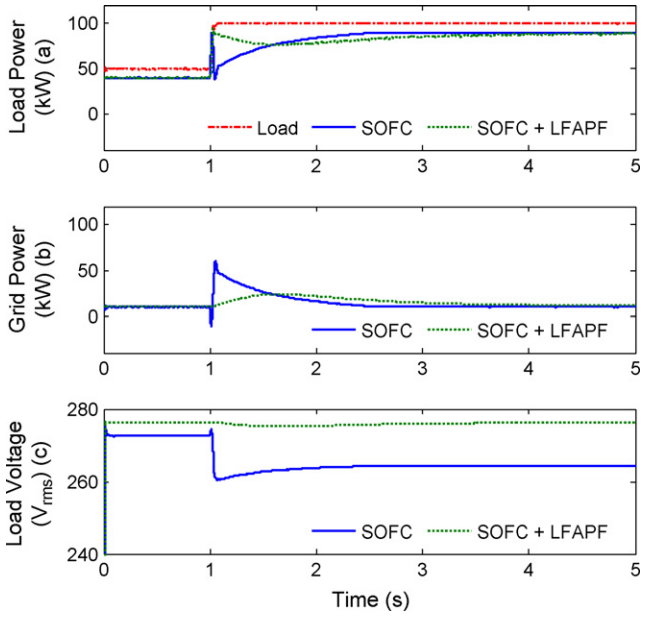

Fig. 13. Load-following SOFC with and without LFAPF during start-up transient.

current in Fig. 12c enables the construction of a more desirable line current which is presented in Fig. 12d with less harmonic distortion. The load-following APF successfully improves the quality of both the line current and the line voltage. This improvement is quantitatively summarized by the voltage and current THD values presented in Table 1. The voltage distortion is roughly 0.7% with the SOFC only, but is a much lower 0.03% with the addition of an LFAPF. The current THD without LFAPF varies from 41% at low load to 10% at high load power, but is always around 4% when paired with an LFAPF. These values are consistent with the qualitative waveform behavior. The LFAPF combined with a base-loaded SOFC model achieves the goals of reducing grid power spikes, reducing voltage sags, and improving voltage and current waveform quality.

4.2. Load-following SOFC

The load-following ability of the LFAPF and SOFC models are illustrated in Fig. 13. Fig. 13a shows the load demand, SOFC power output, and the net power output of the SOFC/LFAPF during the transient power demand increase. The SOFC power jumps up immediately due to stored fuel within the anode compartment, but then quickly falls due to delays in fuel delivery to the stack before slowly rising to eventually meet the power demand after about 1.5 s. The addition of energy storage within the LFAPF allows the combined SOFC/LFAPF power to track the power demand change immediately, although after the initial transient, the SOFC/LFAPF power drops gradually until it meets the actual SOFC power. Then the SOFC/LFAPF combined power falls below the SOFC power, which is due to the control strategy that recharges the LFAPF capacitor. The resulting grid power demands for the case with and without APF are shown in Fig. 13b. Because the LFAPF absorbs the initial load change, the grid power increase is very slight compared to the case without an LFAPF. The LFAPF grid power increases only from 10 to 24 kW while the grid power in the case without an LFAPF temporarily reaches 60 kW.

The load bus benefits from a reduction in the grid power spike associated with the power demand increase because a reduced line current corresponds to less voltage drop. The effect of the load transient on line voltage is presented in Fig. 13c. The case without an LFAPF suffers a voltage sag concomitant with the load increase, while the APF case shows only a slight voltage change. Also, even well after the transient when both cases have the same grid power draw, the case without LFAPF has a lower rms voltage. This is likely due to the reactive power compensation benefit associated with the LFAPF.

The mirror transient perturbation of the early morning start-up transient is the evening shut-down transient, when the power level drops from 100 to 50 kW. The fundamental limiting delay for increasing SOFC power output is the delivery time for additional fuel to reach the anode compartment. When the power demand is decreased, however, the new reference can be met almost immediately by simply reducing the fuel utilization. This means that the power deficit observed in the morning transient will be less noticeable in the evening for the load-following case. The voltage for the SOFC-only case does increase as a result of this transient due to the power quality of the load, but as the LFAPF compensates reactive power and harmonics, the SOFC/LFAPF voltage is uniformly constant throughout the evening transient.

The power quality goals of LFAPF implementation are still met, as presented in the THD comparison of Table 2.

4.3. SOFC offline

Whether the SOFC has load-following ability or not, the installation will inevitably experience times when the SOFC is offline

Table 1
Voltage and current THD for the base-loaded SOFC case.

	50 kW		100 kW	
	SOFC only	SOFC/APF	SOFC only	SOFC/APF
V_{THD}	0.68%	0.025%	0.73%	0.17%
I_{THD}	41%	3.8%	10%	4.0%

Table 2
Voltage and current THD for the load-following SOFC case.

	50 kW		100 kW	
	SOFC only	SOFC/APF	SOFC only	SOFC/APF
V_{THD}	0.68%	0.025%	0.75%	0.035%
I_{THD}	41%	3.8%	15%	4.7%

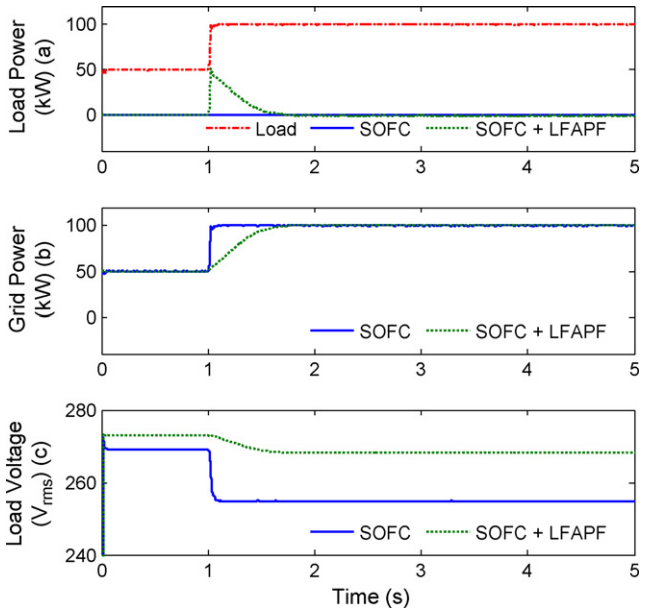

Fig. 14. SOFC offline with and without LFAPF during load increase.

and not actively producing power. This could occur due to an end-user or utility decision, or due to scheduled or unscheduled system maintenance. It is desirable that even under SOFC offline conditions the load can benefit from the LFAPF. To simulate this case the SOFC model physics are removed from the model by setting the generated power to a constant 0 kW.

The dynamic behavior of the SOFC offline system model is similar to that of the base-load SOFC case, since in both cases the load changes but the SOFC power output does not. Thus, the grid power for the SOFC offline case at the morning start-up (Fig. 14) is offset by 40 kW from that of the base-load SOFC case from Fig. 10. The local voltage for both cases also shows a similar trend with a constant offset due to the increased overall current in the SOFC offline case. The evening shut-down power and voltage dynamics for the SOFC offline case equivalently reflect those of the base line case from Fig. 11 and, as a result, are not separately presented herein.

The LFAPF still decreases the THD in both voltage and current, as shown in Table 3. The current THD of the case without APF is lower here than that for the cases with an SOFC, because on-site generation reduces the line current fundamental, and thus increases the magnitude of the harmonics relative to the fundamental.

5. Sensitivity analysis

The results from the previous sections all depend upon the specific feedback gains and the DC capacitor size. A sensitivity analysis of these parameters shows similar trends and behavior, but confirms a strong dependence on the value of the two design parameters.

Table 3
Voltage and current THD for the SOFC offline case.

	50 kW		100 kW	
	No APF	APF	No APF	APF
V_{THD}	0.69%	0.12%	0.72%	0.25%
I_{THD}	18%	3.6%	7.4%	3.5%

Table 4
Relationship of PI values to severity of grid power spike and voltage sag.

	Grid power spike (kW)	Voltage sag (V_{rms})	Min. APF capacitor voltage (V)
High PI	36	2.3	333
Mid PI	24	1.2	269
Low PI	19	0.7	225

Table 5
Current THD for all PI cases during base-load SOFC case.

	Low PI	Mid PI	High PI
I_{THD} (50 kW load)	3.84%	3.84%	3.81%
I_{THD} (100 kW load)	4.02%	4.04%	4.06%

5.1. Feedback gains

The dynamic behavior of the system is compared for a variety of feedback gains used in determining the V_m parameter of the LFAPF. Three sets of PI gains are defined as follows:

Low PI: $P = 0.1$; $I = 0.02$
Mid PI: $P = 1$; $I = 0.2$
High PI: $P = 10$; $I = 2$

The mid PI values were used in all the results from Section 4. As expected, the low PI feedback reduces the tendency of the capacitor to maintain a set voltage, and thus allows it to discharge more fully and accordingly mitigate the magnitude of the grid power spike and load voltage sag. The high PI case impedes capacitor discharge, which tends to exacerbate the severity of the voltage sag and the grid power spike. This is shown in Table 4, where the maximum grid power spike, the voltage sag (difference from initial steady-state) and the minimum voltage the LFAPF DC capacitor reaches are compared for the three PI cases. The high PI case reaches a spike of up to 36 kW, while the low PI only achieves 19 kW from the initial 10 kW. The low PI case also has the smallest voltage sag, and the lowest minimum LFAPF capacitor voltage—falling as low as 225 V when steady-state voltage is 368 V.

As mentioned in Section 4, the base-load SOFC and SOFC offline cases both do not exhibit a distinct grid power spike, but a step load change from one steady-state condition to another. In all PI cases, this transition is affected by the feedback parameters, though the relationship is not as straightforward as in the load-following SOFC situation. For the base-load case response to the morning start-up perturbation, initially the high PI case has the sharpest increase in grid power followed by the mid and then the low PI cases. The low PI case has a reduced slope due to the high rate of energy discharge from the LFAPF capacitor. All cases have the same capacitor size—meaning same total energy storage capacity—and when the low PI case reaches an eventual discharge limit the sudden curtailment causes a steep rise in grid power demand. The low PI case actually reaches the new steady-state condition before the mid PI case, even though it discharges more energy overall, due to this behavior, which is presented along with the associated load voltage behavior and LFAPF capacitor voltage in Fig. 15. The SOFC offline results are similar to those of the base-loaded SOFC.

The current THD is still maintained at about 4% in all PI cases both before and after the transient, as shown in Table 5.

5.2. Capacitor size

The LFAPF DC capacitor size directly affects the amount of energy stored in the LFAPF and the amount of energy that can be injected into the system according to the capacitor energy equation: $E_{cap} = (1/2)CV^2$. A larger capacitor should be more effective,

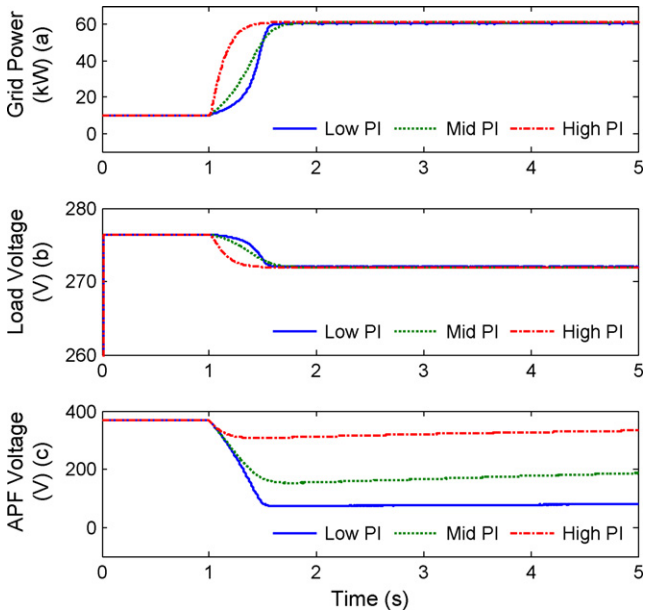

Fig. 15. Base-load SOFC case during start-up transient for various PI feedback parameter values.

and a smaller one less effective. A capacitor size of 300 mF was used in Section 4. Three additional sizes are compared here: 30 mF, 1 F, and 2 F. For the load-following start-up transient, the 30 mF case reaches a momentary grid power demand spike of 45 kW, which is close to that of the no APF condition of 60 kW. The 1 F and 2 F cases reach 16 and 13 kW, respectively (Table 6).

In the base-loaded SOFC case, instead of a distinct grid power spike, the morning start-up transient causes a step power change. Increasing the capacitor size decreases the slope of this transition, as is shown in Fig. 16. The 2 F case succeeds in buffering the transition for 4 s, while the 30 mF case is nearly a step (0.08 s ramp). The behavior of the SOFC offline case is very similar to that of the base-loaded SOFC case.

All capacitor size cases exhibit high power quality, indicating that even small energy storage amounts can produce the desired

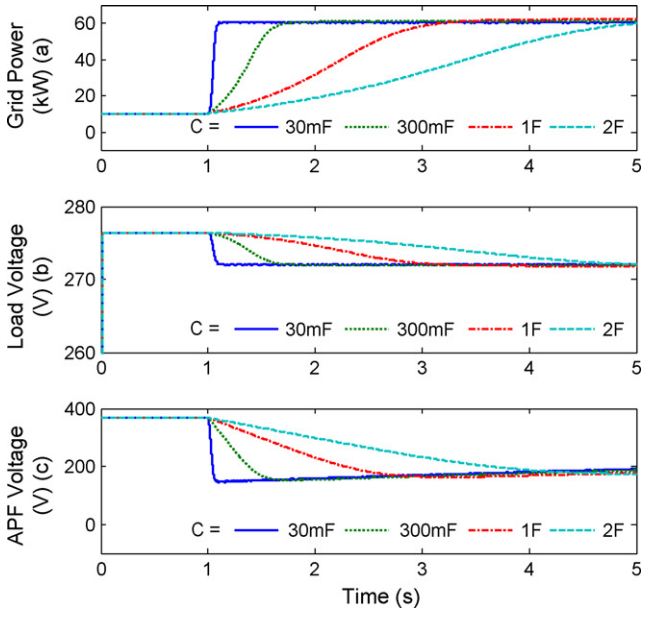

Fig. 16. Base-load SOFC case during start-up transient for multiple LFAPF capacitor values.

Table 6
Relationship of capacitor size to severity of grid power spike and voltage sag during start-up transient.

Capacitance	Grid power spike (kW)	Voltage sag (V_{rms})	Min. APF capacitor voltage (V)
30 mF	45	3.0	182
300 mF	24	1.2	269
1 F	16	0.5	325
2 F	13	0.3	344

Table 7
Current THD for all APF capacitor sizes during base-load SOFC case.

	30 mF	300 mF	1 F	2 F
I_{THD} (50 kW load)	3.81%	3.84%	3.84%	3.84%
I_{THD} (100 kW load)	3.96%	4.04%	4.10%	4.10%

power quality improvements. The current THD at both power levels is presented in Table 7, and is generally about 4% THD in all cases.

6. Conclusions

A design for an OCC load-following active power filter is described and the functionality is demonstrated through implementation in an SOFC system interconnection model. The need for any APF is first identified by simulating a sample interconnection of SOFC and a dynamic non-linear load model that approximates the transient behavior of a commercial office building. While traditional APF systems can achieve many steady-state power quality goals, additional problems associated with load transients persist (e.g., voltage sag). The solution of adding a larger capacitor and reducing the magnitude of feedback gains allows the new LFAPF to provide support during these dynamic conditions as well. The inherent characteristics of OCC control allow the LFAPF to continue meeting the fundamental steady-state control objectives. The case with LFAPF improves harmonic distortion and exhibits a reduction in voltage sag and grid current spike, all of which will improve the power quality of the load and the impact on the utility grid. Some benefit is garnered independent of whether the SOFC has load-following or only base-loaded operating capability, and even whether it is on or offline. The most desirable behavior is achieved when the LFAPF is paired with a load-following SOFC.

The benefits of the LFAPF are the result of a trade-off with the PI feedback parameters and capacitor size. A larger capacitor increases the LFAPF effectiveness, but there is an eventual diminishing benefit versus capacitor cost. Even a relatively small capacitor can succeed in meeting the primary objectives, though it produces less desirable behavior than the other cases with larger capacitors. Changing the PI feedback gains has no associated cost, but optimization is desired: high gains compromise the dynamic capability, while low gains coupled with physical capacitor limitations can produce equally strenuous dynamic responses.

The interconnection of SOFC, load, and electric utility grid requires a delicate balance and set of power electronics components and capabilities to benefit both the end-user and the utility. The use of an LFAPF facilitates this interconnection by (1) augmenting the grid-connected SOFC transient performance capabilities, (2) preventing existing load non-linearity from perturbing the electric utility grid, and (3) enhancing the ability of the external electric utility to provide reliable, high-quality power.

Acknowledgements

The current work was partially supported by the Engineer Research and Development Center of the U.S. Army Corps of Engineers under Contract #: W9132T-08-C-0003 with the Construction

Engineering Research Laboratory. The authors thank Frank Holcomb and Nick Josefik for their technical and administrative support.

References

[1] W.E. Kazibwe, M.H. Sendaula, Electric Power Quality Control Techniques, Van Nostrand Reinhold, New York, New York, 1993.
[2] J.R. Meacham, et al., Journal of Power Sources 156 (2) (2006) 472–479.
[3] B. Singh, K. Al-Haddad, A. Chandra, IEEE Transactions on Industrial Electronics 46 (5) (1999) 960–971.
[4] C. Qiao, T. Jin, K.M. Smedley, Power Electronics Specialists Conference (PESC), Vancouver, BC, Canada, 2001, pp. 1608–1614.
[5] A.E. Auld, et al., Journal of Power Sources 179 (2008) 155–163.
[6] E.M. Guiotto, K.M. Smedley, Industrial Electronics Society IECON, 2003, Roanoke, VA USA, 2003, pp. 1067–1073.
[7] C. Qiao, K.M. Smedley, Industry Applications Conference 2001, Thirty-sixth IAS Annual Meeting, Conference Record of the 2001 IEEE, Chicago, IL, USA, 2001, pp. 2675–2682.
[8] K. Smedley, et al., UCI and Dardel Group First International Conference on Power Electronics for Distributed and Co-generation, Irvine, CA USA, 2004.
[9] J. Wen, K.M. Smedley, M.A. Pai, Advanced Intelligent Mechatronics, Proceedings 2005 IEEE/ASME International Conference, Monterey, CA, USA, 2005, pp. 140–145.
[10] G. Chen, Y. Chen, K.M. Smedley, Applied Power Electronics Conference and Exposition, 2004.
[11] T. Jin, K.M. Smedley, Applied Power Electronics Conference and Exposition, Miami, FL, USA, 2003, pp. 148–153.
[12] K. Smedley, S. Cuk, IEEE Transactions on Power Electronics 9 (4) (1994) 405–413.
[13] M.C. Williams, J.P. Strakey, S.C. Singhal, Journal of Power Sources 131 (2004) 79–85.
[14] M.C. Williams, J.P. Strakey, W.A. Surdoval, Journal of Power Sources 143 (2005) 191–196.
[15] M.C. Williams, et al., Solid State Ionics 177 (2006) 2039–2044.
[16] W.A. Surdoval, Power and Energy Society General Meeting — Conversion and Delivery of Electrical Energy in the 21st Century, 2008 IEEE, 2008.
[17] J.E. Brown, C.N. Hendry, P. Harborne, Energy Policy 35 (4) (2007) 2173–2186.
[18] A.E. Auld, et al., 39th North American Power Symposium 2007. NAPS'07, 2007.
[19] F. Mueller, et al., Journal of Fuel Cell Science and Technology 3 (2) (2006) 144–155.
[20] F. Mueller, Mechanical and Aerospace Engineering, University of California, Irvine, 2005, p. 141.
[21] R. Roberts, J. Brouwer, Journal of Fuel Cell Science and Technology 3 (2006) 18–25.
[22] F. Mueller, et al., Journal of Fuel Cell Science and Technology (2007).
[23] R. Roberts, Mechanical and Aerospace, University of California, Irvine, 2005, p. 338.
[24] F. Mueller, et al., Journal of Power Sources 172 (1) (2007) 308–323.
[25] F. Mueller, et al., Journal of Power Sources 176 (1) (2008) 229–239.
[26] J. Brouwer, et al., Journal of Power Sources 158 (1) (2006) 213–224.
[27] K. Min, et al., 4th International Conference on Fuel Cell Science, Technology and Engineering, Irvine, CA, 2006.
[28] F. Mueller, F. Jabbari, J. Brouwer, Journal of Power Sources 187 (2) (2009) 452–460.
[29] P. Beckhaus, et al., Journal of Power Sources 127 (2004) 249–299.
[30] T.J. Pukrushpan, G.A. Stefanopoulou, P. Huei, in: J.M. Grimble, A.M. Johnson (Eds.), Advances in Industrial Control, Springer, London, 2005.
[31] R. Gaynor, et al., Journal of Power Sources 180 (1) (2008) 330–342.
[32] R.C. Kryter, H.D. Haynes, Seventh Power Plant Dynamics Control and Testing Symposium, Knoxville, TX, May 15–17, 1989.
[33] A.G. Ivanov, I.I. Ushakov, Russian Electrical Engineering 78 (10) (2007) 532–536.
[34] G.D. Marques, Industrial Electronics Society IECON'98. Proceedings of the 24th Annual Conference of the IEEE, Lisboa, Portugal, 1998.